Relationships between climate, vegetation, and energy exchange across a montane gradient

Ray G. Anderson[1,2] and Michael L. Goulden[1]

Received 8 July 2010; revised 3 November 2010; accepted 3 January 2011; published 10 March 2011.

[1] We measured the evaporative fraction (EF) across a semiarid elevation gradient in the San Jacinto and Santa Rosa Mountains of southern California using the Regional Evaporative Fraction Energy Balance platform and four eddy covariance towers. We compared our measurements to precipitation estimates and satellite observations of vegetation indices to assess the seasonal and interannual controls of precipitation and vegetation on surface energy exchanges. Precipitation amount and timing had the largest effect on evaporative fraction, with vegetation having a relatively greater importance at higher elevations than lower elevations. Vegetation cover was linearly related to mean annual EF, but did not predict seasonal variation in EF in most of the study area's ecosystems. Multiyear vegetation observations show that vegetation density increases in a stepwise pattern with precipitation, probably due to shifts in dominant plant communities. Precipitation is a more important factor in controlling EF than temperature. Possible future climate change, including decreases in precipitation amount and increases in variability, could decrease vegetation cover, thus reducing EF and increasing albedo.

Citation: Anderson, R. G., and M. L. Goulden (2011), Relationships between climate, vegetation, and energy exchange across a montane gradient, *J. Geophys. Res.*, *116*, G01026, doi:10.1029/2010JG001476.

1. Introduction

[2] Patterns of vegetation distribution and energy exchange are crucial because they control regional climate [*Beringer et al.*, 2005; *Hogg et al.*, 2000; *Wendt et al.*, 2007], ecosystem water yield [*Huxman et al.*, 2005; *Molotch et al.*, 2009], and are closely linked to ecosystem productivity [*Law et al.*, 2002; *Veenendaal et al.*, 2004; *Scott et al.*, 2009]. In turn, energy partitioning and evaporation are affected by climate and vegetation, thus resulting in a potential feedback loop. Anthropogenic factors are expected to cause future changes in regional climates [*Karl and Trenberth*, 2003; *Diffenbaugh et al.*, 2008], with associated changes in vegetation type, density and structure [*Betts et al.*, 1997; *Cramer et al.*, 2001]. Significant anthropogenic changes in regional climate have already been observed during the latter half of the twentieth century [*Bonfils et al.*, 2008; *Pierce et al.*, 2008; *Hidalgo et al.*, 2009]; leading to widespread, regional impacts on ecosystems [*Breshears et al.*, 2005; *van Mantgem and Stephenson*, 2007; *Kelly and Goulden*, 2008].

[3] Mountains are important to regional hydrology and ecology. Mountains often receive more precipitation than surrounding lowlands due to orographic effects; thus they act as "water towers" in storing and providing water to downstream ecosystems and users [*Viviroli and Weingartner*, 2004]. Mountains act as "Sky Islands," providing cooler temperatures and more available water for isolated ecosystems. Mountains may also be more sensitive to future climate change than other ecosystems [*Messerli et al.*, 2004]. Moreover, some water-limited regions (e.g., the southwestern United States) may see a large decrease in precipitation [*Seager et al.*, 2007; *Diffenbaugh et al.*, 2008]. Changes in atmospheric circulation may alter storm tracks thus leading to large shifts in precipitation and affiliated ecosystem impacts.

[4] One example of the importance of mountains to regional water supplies and ecosystems is found in southern California. Southern California's mountains provide water for urban and suburban areas and have important recreational value [*U.S. Department of Agriculture* (*USDA*), 2007]. Ecosystem shifts in southern California's mountains are likely to be of economic and societal importance. These mountains also lie at "urban-wildland fire interfaces," where human activities have increased the frequency of wildfire [*Syphard et al.*, 2007], which can act as agent of ecosystem change [*Scheffer et al.*, 2001]. Urbanization near these mountains may have already lead to regional temperature increases [*LaDochy et al.*, 2007] that could affect mountain evaporation and/or energy exchange by increasing potential evapotranspiration. Understanding the current relationship between precipitation, energy partitioning, and vegetation in montane regions is key to predicting the effects of future climate change on regional ecosystems and hydrology.

[5] While mountains are important to regional hydrology, current methods to assess evaporation and energy exchange

[1]Department of Earth System Science, University of California, Irvine, California, USA.
[2]University of California Center for Hydrologic Modeling, University of California, Irvine, California, USA.

0148-0227/11/2010JG001476

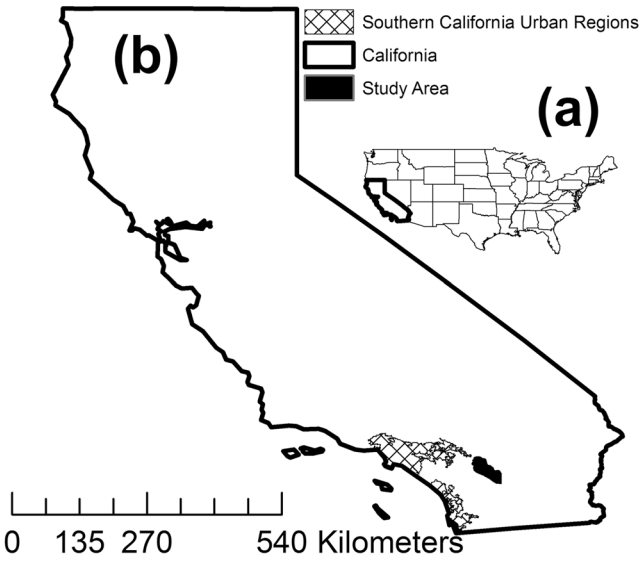

Figure 1. (a) Map of California in relation to the conterminous United States. (b) Map of San Jacinto/Santa Rosa Mountains (study area) in relation to the state of California and southern Californian conurbations. Major metropolitan regions include Los Angeles/Orange/Riverside/San Bernardino Counties (west-northwest of study area) and San Diego (southwest of study area).

are less developed and accurate in these heterogeneous areas. Satellite approaches to estimate regional evapotranspiration do not work well because they rely on gradients of radiometric temperatures and/or vegetation indices to estimate evaporative fraction (EF) and Evapotranspiration (ET) based on empirical relationships; these relationships are confounded by elevation effects [*Li et al.*, 2009]. Commonly used approaches, such as the Temperature-Vegetation Triangle Index or surface energy balance algorithms, require flat surfaces [e.g., *Bastiaanssen et al.*, 1998; *Carlson*, 2007]. Site-specific approaches, such as scaling eddy covariance towers, are limited by sampling density and ecosystem heterogeneity. Larger-scale sampling approaches such as scintillometry [*Ezzahar et al.*, 2007; *Kleissl et al.*, 2009] can assess wider spatial averages of latent heat fluxes from residuals of net radiation, ground heat flux, and sensible heat flux, but these methods obscure spatial patterns.

[6] In this study, we use a new method, the Regional Evaporative Fraction Energy Balance (REFEB), in conjunction with satellite vegetation observations and gridded meteorological data to assess the patterns of energy exchange across elevation transects in southern California. We used satellite vegetation indices to stratify sampling by ecosystem class and measured evaporative fraction (EF), the fraction of available energy (net radiation minus ground heat flux) that is used to evaporate water, across the gradient at monthly intervals. We then evaluated vegetation indices' capability to predict ecosystem EF at various timescales. Finally, we examined the climate-vegetation linkages across the gradient that affects EF.

2. Methods

2.1. Study Area

[7] The study area is in the San Jacinto and Santa Rosa Mountains of southern California (Figure 1, hereafter referred to as "study area"). The area is 1,461 km^2, and elevations range from ~10 m asl at the base of the desert foothills on the eastern (leeward) side of the mountains to ~3300 m at the summit of San Jacinto Peak (National Geodetic Survey, database datasheets available at http://www.ngs.noaa.gov/, 2009). Most of the study area is within the San Jacinto State Park and Wilderness, the San Bernardino National Forest, or lands administered by the Bureau of Land Management. The study area is primarily used for recreation, though it is an important water source for the cities of Hemet and Palm Springs. We excluded areas of the San Jacinto Mountains burned by the 2006 Esperanza Fire, a large (~16,000 ha), intense wildfire (California Fire Resource and Assessment Program, fire perimeter data available at http://frap.cdf.ca.gov/, 2009). The study area includes significant amounts of five International Geosphere-Biosphere Programme (IGBP) vegetation classes (Table 1; the 500 m, annual resolution IGBP classification product from the Moderate Resolution Imaging Spectroradiometer (MODIS), product ID: MCD12Q1) [*Friedl et al.*, 2002].

[8] The study area is a good locale for examining the impact of vegetation and climate on energy partitioning as it is undergoing rapid ecological shifts that mirror many larger current and predicted trends in the western United States. The area has steep climate and vegetation gradients (Figures 2 and 3). In a ~2300 m elevational transect in the Santa Rosa Mountains, *Kelly and Goulden* [2008] found

Table 1. IGBP Classifications

Anderson and Goulden ENVI Classification[a]	IGBP Classification[b]				
	ENF (1)	CS (6)	OS (7)	S (8)	C (14)
Lower Sonoran Desert (LowDes or LD)	0	8	90	0	0
Upper Sonoran Desert (HiDes or HD)	0	30	68	0	0
Grassland (Grass or G)	0	14	83	0	0
Open Shrubland (Oshrub or OS)	2	59	33	5	0
Dry Chaparral and Pine Forest (DryChap or DC)	0	71	12	15	0
Medium Chaparral and Pine Forest (MedChap or MC)	4	58	4	33	0
Mixed Chaparral, Live oak, and Conifer (Mixed or M)	9	25	3	59	0
Deciduous Oak and Conifer (Doak or DC)	15	29	1	51	0
Live Oak and Conifer (Evergreen or E)	4	12	3	69	5

[a]Hereafter often referred to by class abbreviation for brevity.
[b]Classifications are as follows: 1, Evergreen Needleleaf Forest; 6, Closed Shrublands; 7, Open Shrublands; 8, Woody Savannahs; 14, Cropland/Natural vegetation mosaic.

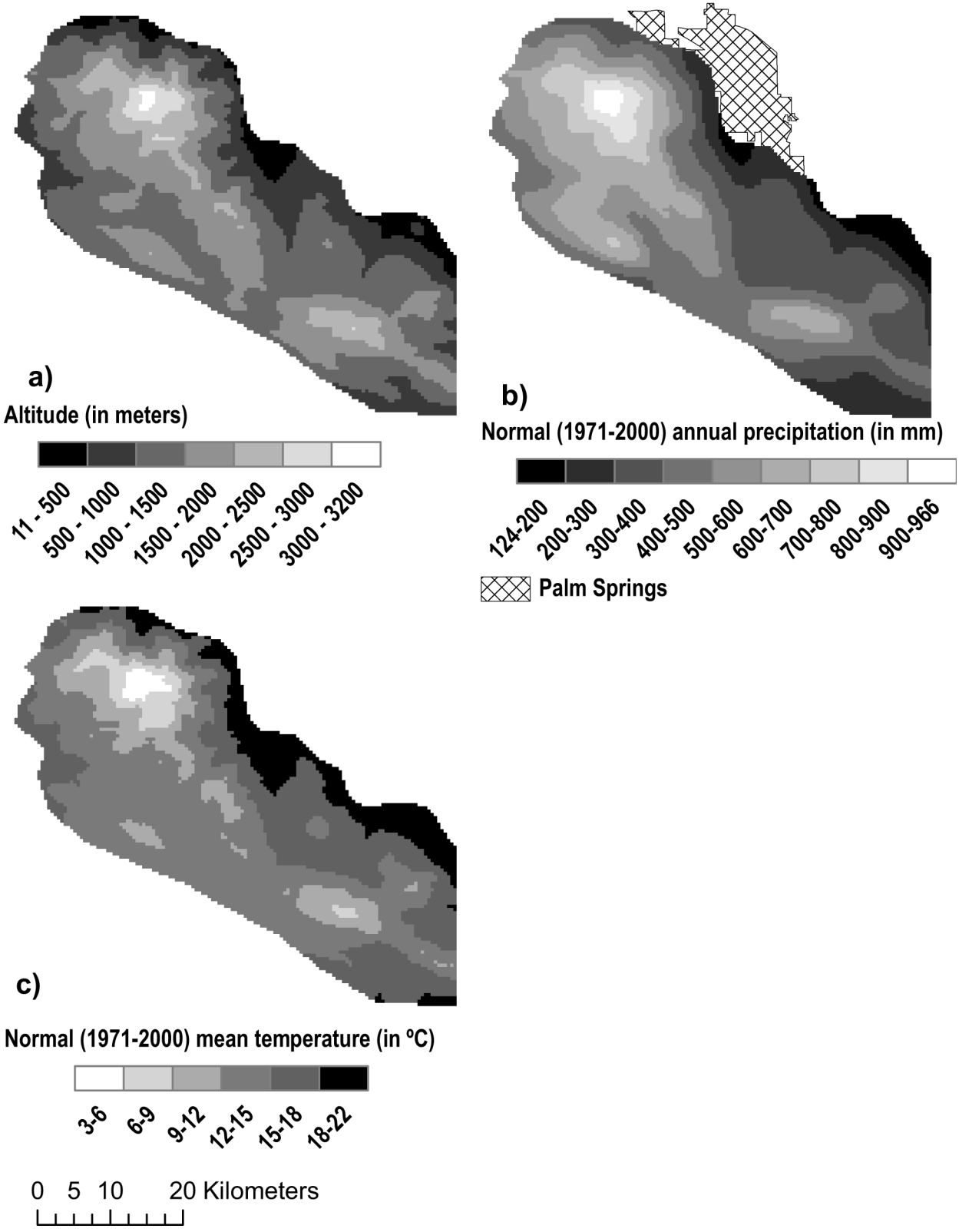

Figure 2. Study area maps of (a) elevation, (b) normal (1971–2000) precipitation, and (c) normal temperature. Elevation, precipitation, and temperature data comes from 800 m normal data from PRISM. EVI is mean of 16 day MODIS images used to develop classification in Figure 3. Precipitation and EVI data were resized to 0.00405600° grids. Normal precipitation increases with elevation and windward aspect. For scale and location reference, the city limits of Palm Springs, California, are shown in Figure 2b.

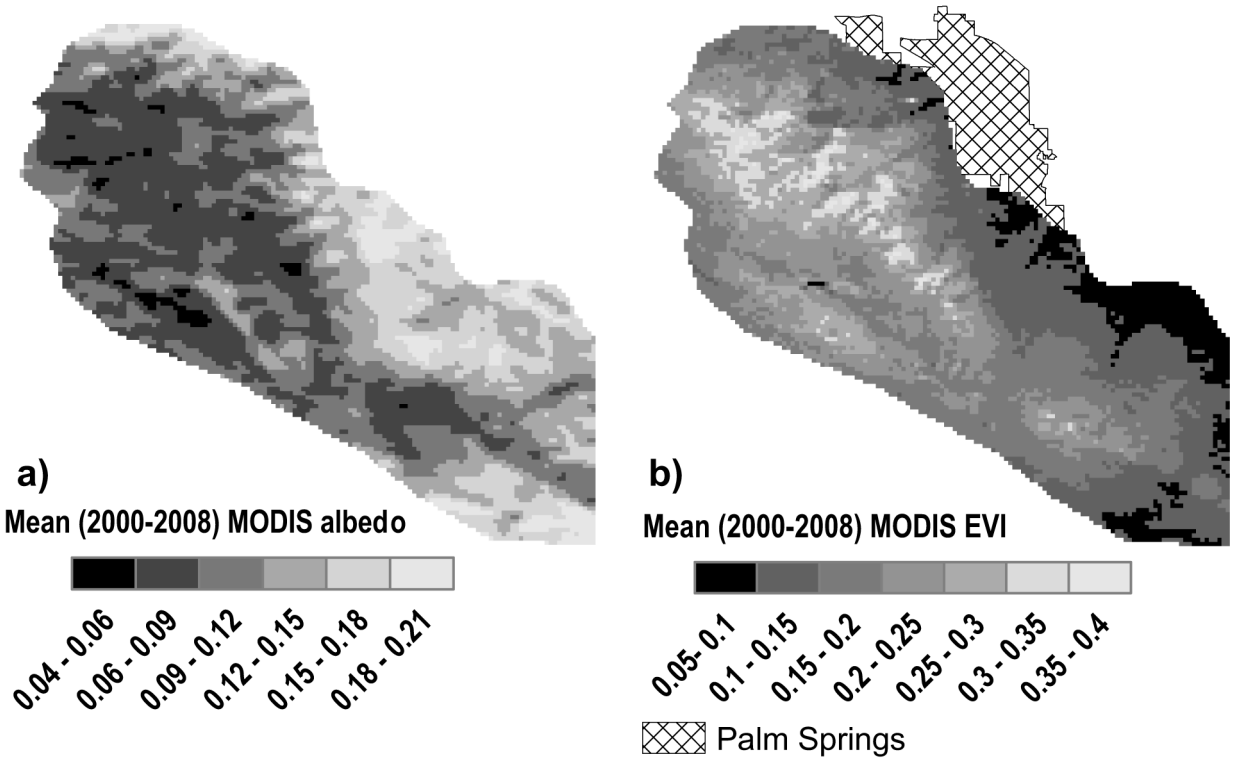

Figure 3. Study area maps of average (2000–2008) MODIS (a) albedo and (b) EVI. EVI is mean of 16 day MODIS images used to develop classification in Figure 3. Albedo is mean of 8 day images from same time period as EVI observations. EVI and albedo were resized to 0.00405600° grids. EVI generally increases with elevation and west aspect with the highest mean EVI values found in windward facing, high-altitude (1500–2500 m) valleys and canyons. Albedo is well correlated with EVI, with lowest albedos in windward high-altitude valleys and highest albedo in low-elevation, leeward deserts. For scale and location reference, the city limits of Palm Springs, California, are shown in Figure 3b.

that average plant distributions moved up ~65 m in elevation over the past 30 years. Precipitation variability and near-surface temperature increased and snow cover decreased during this time. A recent outbreak of bark beetles killed a large number of trees at middle and higher elevations in the study area, resulting in concerns over more intense wildfires and the implementation of thinning programs to reduce tree density [*USDA*, 2007]. The study area lies in an urban-wildland interface that experiences increased fire incidence and considerable twentieth century forest fire suppression [*McKelvey et al.*, 1996; *Keeley et al.*, 1999].

2.2. Satellite Vegetation and Spatially Modeled Precipitation and Temperature

2.2.1. Precipitation and Temperature Data

[9] Precipitation and temperature come from the Parameters Regression Independent Slopes Model (PRISM) group (PRISM Climate Group, Oregon State University, data available at http://www.prismclimate.org/, 2009). PRISM incorporates a spatial interpolation model that explicitly considers the effect of topography on climate, a crucial consideration since the study area has less than five long-term weather stations and complex and rugged topography. We used the 4 km gridded monthly/annual precipitation data and the 800 m 1971–2000 normal monthly precipitation and mean maximum and minimum temperatures.

[10] We used two sources to evaluate the uncertainty in the gridded PRISM data. First, we compared PRISM monthly precipitation, monthly mean minimum temperature, and monthly maximum temperature to three meteorological stations managed by the University of California's Phillip J. Boyd Deep Canyon Desert Research Center. These three stations are not included in the PRISM interpolation. Table 2 shows uncertainty in PRISM data as compared to these three stations. The agreement between monthly precipitation/temperature at the gauges and the PRISM value was good, with a coefficient of determination (r^2) at least 0.85 in all cases. Maximum temperature had better agreement than minimum temperature, which indicates that PRISM may not fully capture cold air drainage in the study area. We believe the precipitation agreement is encouraging given that the three gauges (1) are on the leeward side of the study area, (2) span a vertically gradient larger than 1000 m, and (3) lie near a canyon with vertical relief approaching 1000 m. Our second source is a USGS publication [*Jeton et al.*, 2005] evaluating uncertainty in the 800 m resolution precipitation climatological product over Nevada. *Jeton et al.* [2005] concluded that the mean uncertainty in PRISM precipitation was ±15% over Nevada. Considering that the mean precipitation in Nevada is less than 250 mm yr^{-1}, this shows that the absolute error in PRISM precipitation is relatively small.

Table 2. Assessment of PRISM Error by Comparison of PRISM Values for Three Stations Not Included in PRISM Interpolation (University of California Phillip Boyd Deep Canyon Research Center, Unpublished Data, 2010)

	Site		
Parameter	Pinyon Crest	Agave Hill	Boyd Campground
Latitude (°N)	33.61197	33.63891	33.67028
Longitude (°W)	116.43772	116.39833	116.36744
Altitude (m)	1244	835	207
Calendar years	1982–2009	1974–2009	1982–2009
Monthly Precipitation (P) Slope	0.82	1.20	1.04
P R^2	0.88	0.86	0.85
P Mean Absolute Error (MAE) (mm $month^{-1}$)	11.47	7.76	3.04
Minimum Temperature (Min T) Slope	0.80	0.83	1.02
Min T y-intercept (°C)	−1.10	−3.60	−4.06
Min T R^2	0.93	0.92	0.97
Min T MAE (°C)	3.61	6.38	3.79
Max T Slope	0.91	0.98	1.00
Max T y-intercept (°C)	2.17	0.64	−1.49
Max T R^2	0.88	0.96	0.98
Max T MAE (°C)	1.93	1.41	1.52

2.2.2. Satellite Observations

[11] Vegetation observations come from the 250 m, 16 day resolution Enhanced Vegetation Index (EVI) from MODIS (product ID MOD13Q1 v5) [*Huete et al.*, 2002]. We used EVI to create vegetation classes for sampling (see section 2.3) and to relate our EF measurements to vegetation cover. We used EVI as a vegetation proxy in evaluating the relationships between vegetation, EF, and precipitation. We extracted individual pixel records of EVI for each eddy covariance (EC) tower and mobile measurements. EVI values for individual mobile and tower measurements were used if they contained a nonfill value.

[12] Albedo observations were derived from the MODIS 500m, 16 day Nadir-BRDF adjusted reflectance (product ID MCD43A4 v5) [*Schaaf et al.*, 2002]. Shortwave, broadband albedo was calculated from band reflectances following *Liang et al.* [2002]. Prior to analysis, all spatial data were reprojected to congruent 0.00405600° by 0.00405600° cells using the cubic convolution algorithm in The Environment for Visualizing Images (ENVI) software (version 4.2, Research Systems Inc., Boulder, CO).

2.3. Mobile Sampling Design and Measurements

[13] We classified the study area into vegetation classes to ensure representative sampling. To create classes, we took EVI 16 day composites from day 49 of year 2000 (the beginning of the MOD13Q1 record) till day 265 of 2008. We used ENVI to group study area pixels with the unsupervised IsoData classification algorithm [*Tou and Gonzalez*, 1974]. We specified nine classes, a 1% change threshold, 100 maximum iterations, and left all other default options in place. The IsoData algorithm grouped each class by mean EVI, seasonality, and interannual variation; pixels that had similar 9 year time series were grouped in the same class. We used nine classes because this number of classes allowed convenient road access to multiple sampling locations while still enabling class differentiation to stratify sampling. MODIS has been shown to successfully differentiate vegetation types across other Mediterranean climate gradients, despite the difficulties of using vegetation indices in these regions [*Evrendilek and Gulbeyaz*, 2008].

[14] We conducted two types of surveys to assess the specific types of vegetation in each class. We compared our ENVI vegetation classification to the modal IGBP classification from 2001 to 2007. Additionally, we surveyed each class in October 2009, visiting six locations in each class that overlapped with our REFEB sampling. At each location, we measured a transect that was directed into the dominant wind direction, starting at 10 m from the truck and progressing to 60 m. Every 5 m we sampled leaf area index (LAI) using a light sensor (LAI-2000, Licor Inc., Lincoln, NE, USA) and visually classified each 5 m for a total of 10 LAI and vegetation samples. Visual vegetation classes were nonvegetated, grass, deciduous shrub, evergreen shrub, deciduous oak, evergreen oak, or conifer. In some locations (<20), steepness of terrain and/or density of vegetation made a full 60 m transect upwind unsafe or unfeasible. In these locations, we sampled along a transect parallel to the road and truck to obtain 10 LAI and vegetation samples. Mean LAI and visual plant classifications are presented in Table 3.

[15] We made monthly REFEB measurements for the 2008–2009 water year (October 2008 to September 2009). For each campaign we tried to make six measurements per class for a total of 54 measurements per month. Sampling locations were selected so that the prevailing wind direction was into the truck and the majority of the flux footprint had canopies below the height of the REFEB instrumentation. Most measurements were made along five dirt and two paved roads within the study area (Figure 4). These routes were chosen to balance sampling efficiency while sampling all classes equally. We also sought to balance the number of measurements on the windward (western) and leeward (eastern) slopes for vegetation classes with significant presence on both slopes.

Table 3. Average Percent Vegetation Cover for Each ENVI Class From Survey Transects

Class	LAI	Deciduous Shrub or Grass	Evergreen Shrub	Deciduous Oak	Evergreen Oak	Conifer	Nonvegetated	Succulent
LowDes	0.64	27	13	0	0	0	58	2
HiDes	1.14	31	23	0	0	0	42	5
Grass	1.37	66	14	0	0	0	15	5
Oshrub	1.15	13	33	0	0	8	37	9
Dry Chap	2.38	19	50	0	7	10	14	0
Med Chap	2.69	11	48	0	7	23	11	0
Mixed	2.26	3	10	0	40	29	18	0
Doak	2.04	2	9	45	23	17	5	0
Evergreen	2.29	5	11	0	50	16	18	0

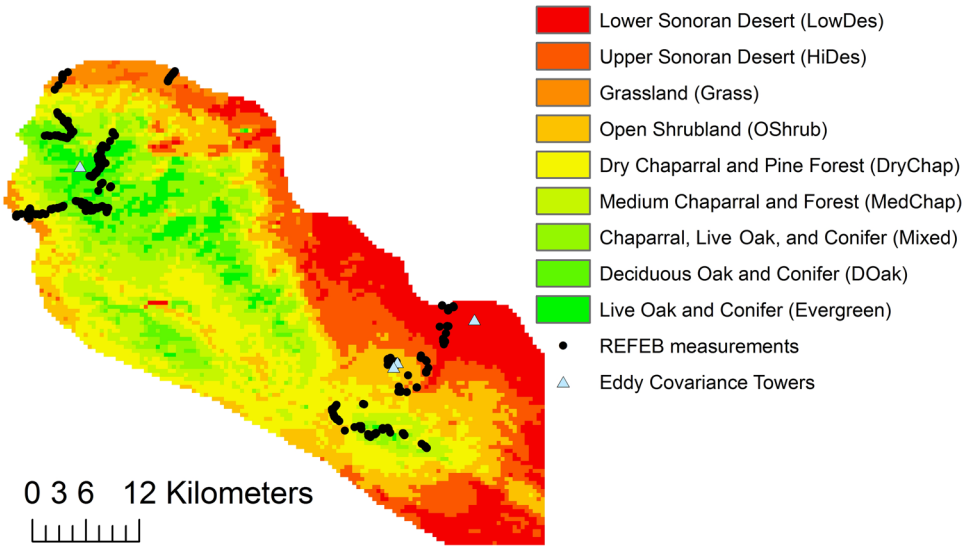

Figure 4. Map of study area showing REFEB sampling locations, eddy covariance towers, and ENVI IsoData vegetation classification. Visual vegetation class description and number are given for each class.

2.4. Eddy Covariance

[16] Four eddy covariance (EC) towers were established in the study area in 2006 (Table 4). Tower instruments and flux processing details can be found in the works of *Goulden et al.* [2006] and *McMillan et al.* [2008]. We did not gap fill missing tower data and considered only daytime measurements (half-hour EF between 0 and 1 and net radiation >10 W m^{-2}) with sufficient turbulence (friction velocity >0.1 m s^{-1}). We used PRISM precipitation for all sites because the Deciduous Oak/Conifer tower lacked sufficient instrumentation to accurately capture snowfall, which contributes a considerable percentage of site precipitation at this site. Monthly EF at each tower was calculated by averaging all valid daytime half-hour tower measurements.

2.5. Mobile REFEB Platform

[17] We used the Regional Evaporative Fraction Energy Balance (REFEB) platform to make 10 min measurements of evaporative fraction (EF). Details about REFEB instrumentation and theory are provided by *Anderson and Goulden* [2009]. REFEB uses an InfraRed Gas Analyzer (IRGA) to measure CO_2 and H_2O and a sonic anemometer to measure temperature (T), all at 10 Hz. CO_2 and H_2O mixing ratios are expressed per mole dry air. Using *Rannik and Vesala*'s [1999] approach, we then detrend the mean component of each of the measurements to obtain the fluctuating component (e.g.,$T' = T - \overline{T}$ and $H_2O' = H_2O - \overline{H_2O}$). H_2O vapor concentrations are converted into specific humidity fluctuations (q′).

[18] Evaporative fraction (EF) is defined as the fraction of energy used to evaporate water (equation (1))

$$EF = \frac{LE}{AE} = \frac{LE}{(Rn - G)} \tag{1}$$

where LE is latent heat flux, AE is available energy, Rn is net radiation, and G is ground heat flux. EF can also be derived directly from T′ and q′ measurements using the Regression Bowen Ratio approach of *De Bruin et al.* [1999] as shown in equation (2).

$$EF = \frac{1}{1 + \gamma\left(T'/q'\right)} \tag{2}$$

where γ is the psychrometric constant.

[19] The instruments are mounted on a truck that is parked downwind of a sampling area for 10 min to obtain enough data for a regression. While REFEB was chosen primarily for its mobile sampling capability, it also has an advantage over eddy covariance in not requiring coordinate rotation, which can be a significant source of error in complex topography [*Turnipseed et al.*, 2003]. REFEB is also advantageous because net radiation and ground heat flux estimates are not needed at the measurement locations to determine EF and plant water use efficiency (WUE).

[20] Our instrumentation was identical to that of *Anderson and Goulden* [2009] with the exception that we added a

Table 4. Site Information for the Four Eddy Covariance Towers in the Study Area

Tower Description by ENVI Vegetation Class	Latitude	Longitude	Elevation (m)	Date Established
Low Sonoran Desert	33°39′10″N	116°22′21″W	300	23 Apr 2006
Disturbed Open Shrubland[a]	33°36′34″N	116°27′02″W	1294	6 May 2006
Undisturbed Open Shrubland	33°36′17″N	116°27′16″W	1292	18 May 2006
Deciduous Oak and Conifer	33°48′29″N	116°46′18″W	2057	11 Sep 2006

[a]Disturbed Open Shrubland tower footprint area burned in a 1994 fire.

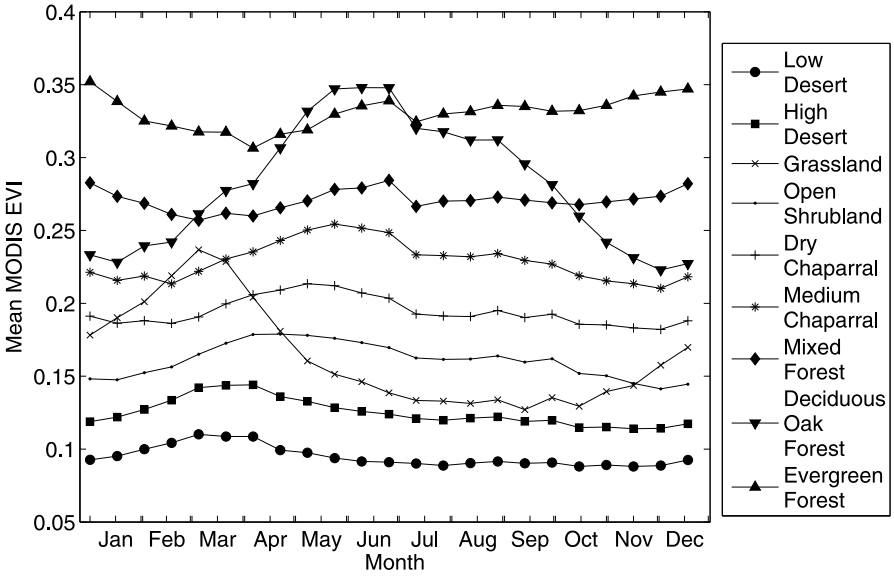

Figure 5. Mean seasonal 16 day MODIS EVI for each ENVI classification (Figure 4). MODIS data averaged from the beginning of MODIS record (day 49 of year 2000) to day 265 of year 2008.

closed path IRGA (Li-7000, Licor Inc., Lincoln, NE, USA), a brushless air pump (MPU 1046-N815-3.99, KNF Neuberger Inc., Trenton, NJ, USA), and a 2 m plastic tube (Bev-A-Line IV, Thermoplastic Processes, Georgetown, DE, USA). We added these instruments after observing larger fluctuations in q′ with an open path IRGA than with a closed path IRGA in a preliminary test. We hypothesized that the added fluctuations were due to significantly lower water vapor concentrations and fluctuations present in the study area, compared to the region used by *Anderson and Goulden* [2009]. This error would be amplified in regions (such as the study area) with large sensible heat fluxes, larger density corrections, and possible contamination of the open-path window [*Serrano-Ortiz et al.*, 2008]. Closed path IRGAs have less uncertainty in the air density correction necessary to obtain fluctuations in CO_2 and H_2O concentrations. We determined the closed path lag by maximizing the correlation between the two IRGAs and then used this lag to synchronize the closed path IRGA and sonic anemometer observations. For all campaigns the lag was 0.3 s.

[21] We used the same quality control and filtering algorithm as *Anderson and Goulden* [2009], with the additional constraint of rejecting data where EF was greater than 1. This was because a primary cause of this condition (the Oasis Effect) is not present in the study area whereas it is common in *Anderson and Goulden*'s [2009] study region; thus EF greater than 1 in the study area indicated an erroneous measurement. We used EF calculated by the open-path IRGA to gap fill some samples (<20 of 675) where the closed path IRGA was not working properly. To do this, we used points where both the open and closed path IRGAs measured acceptable EF and WUE values. We regressed closed path versus open path EF measurements and applied the resulting equation to the open path EF value to fill the erroneous closed path EF measurement. The differences between the open and closed path EF were small (Data Set S1, available as auxiliary material).[1] The regression between closed and open path IRGAs had a coefficient of determination (r^2) of 0.98, slope of 1.03, and intercept of less than 0.01. The good agreement between IRGAs indicates that fluctuations in open path IRGA measurements were considerably less than suggested by our preliminary tests.

3. Results

3.1. Topography, Climate, and Vegetation Distribution

[22] Elevation, normal temperature, annual precipitation, MODIS EVI, and MODIS albedo are well correlated (Figures 2 and 3). Elevation ranges from near sea level to more than 3,000 m with most of the study area above 1,500 m (Figure 2a). Normal (1971–2000) mean annual temperature varies from 3 to 21°C while normal annual precipitation varies from 125 mm to 965 mm (Figures 2c and 2b). Mean EVI ranges from 0.06 to 0.40, with the lower extreme indicating an almost complete lack of vegetation in some pixels (Figure 3b). The highest EVI values occurred in higher altitude (1500–2500 m) drainages on the windward (western) slope. Albedo ranges from 0.05 to 0.21 and is inversely related to EVI (Figure 3a).

[23] Vegetation classes (Figure 4) track mean annual EVI and EVI seasonality (Figure 5). Mean class EVI ranges from ~0.1 for the Low Sonoran Desert to ~0.33 for the Live Oak and Conifer class. The timing of peak EVI ranges from March for the lower-elevation classes to June and July for the highest-elevation classes (Figure 5). Most classes are dominated by evergreen species and show relatively little seasonal variation in EVI; however, the Grassland and Deciduous Oak show clear greening and senescence because they consist of a mix of evergreen and deciduous vegetation.

[1] Auxiliary materials are available at ftp://ftp.agu.org/apend/jg/2010jg001476.

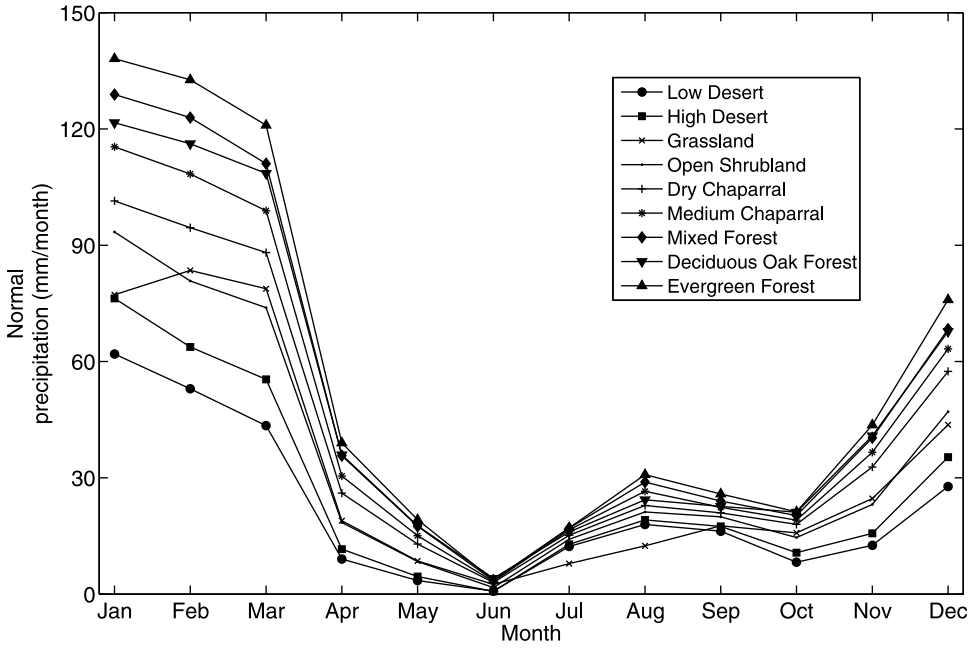

Figure 6. Mean monthly normal (1971–2000) precipitation for each of the vegetation classes from the ENVI algorithm. January has the highest precipitation for all classes except grassland while June has the lowest. A monsoon occurs in August and September with a decrease in fall precipitation before winter storms resume. Averaged by class, precipitation shows a strong positive relationship with mean class EVI.

[24] Our vegetation classes showed consistent patterns when compared with the MODIS land cover product and our own field survey (Tables 1 and 3). Our lower-elevation classes (Desert and Grasslands) were primarily classified into the Open Shrubland IGBP class by MODIS (Table 1). Classes found at intermediate precipitation (Open Shrubland and Chaparral) were primarily classified as Closed Shrubland, while highest-precipitation classes (Mixed, Oak and Conifer) were classified as Woody Savanna. With the visual survey, our classes were stratified by LAI, with LAI greater than 2 for Chaparral and wetter classes and LAI less than 1.6 for all other classes (Table 3). Plant cover shifted

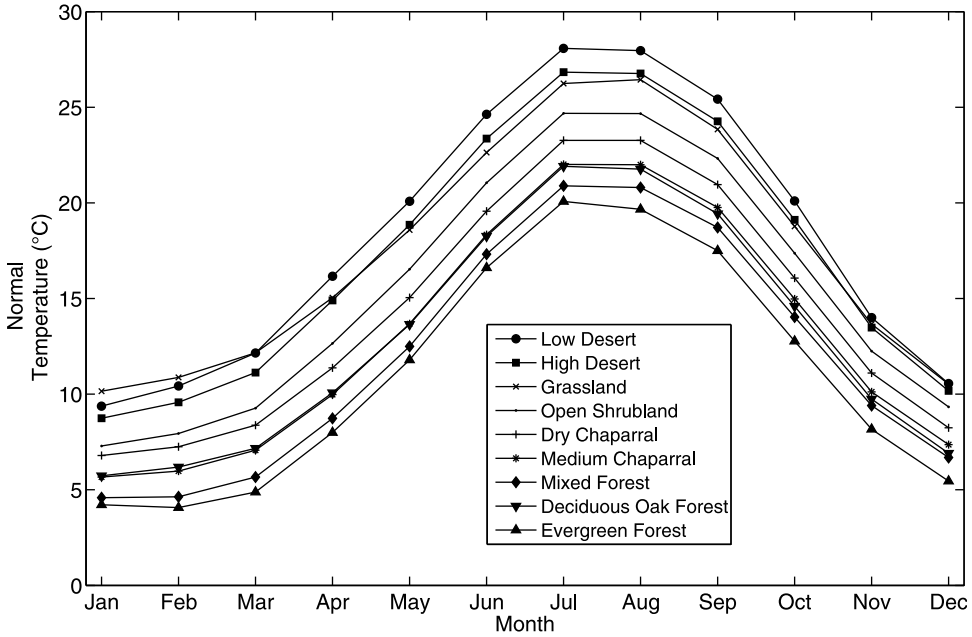

Figure 7. Mean monthly normal (1971–2000) temperature for each of the ENVI vegetation classes. Mean monthly temperature patterns for each class parallel each other well with the exception of the Grassland and Mixed classes, which vary in their relative temperature rank throughout the year.

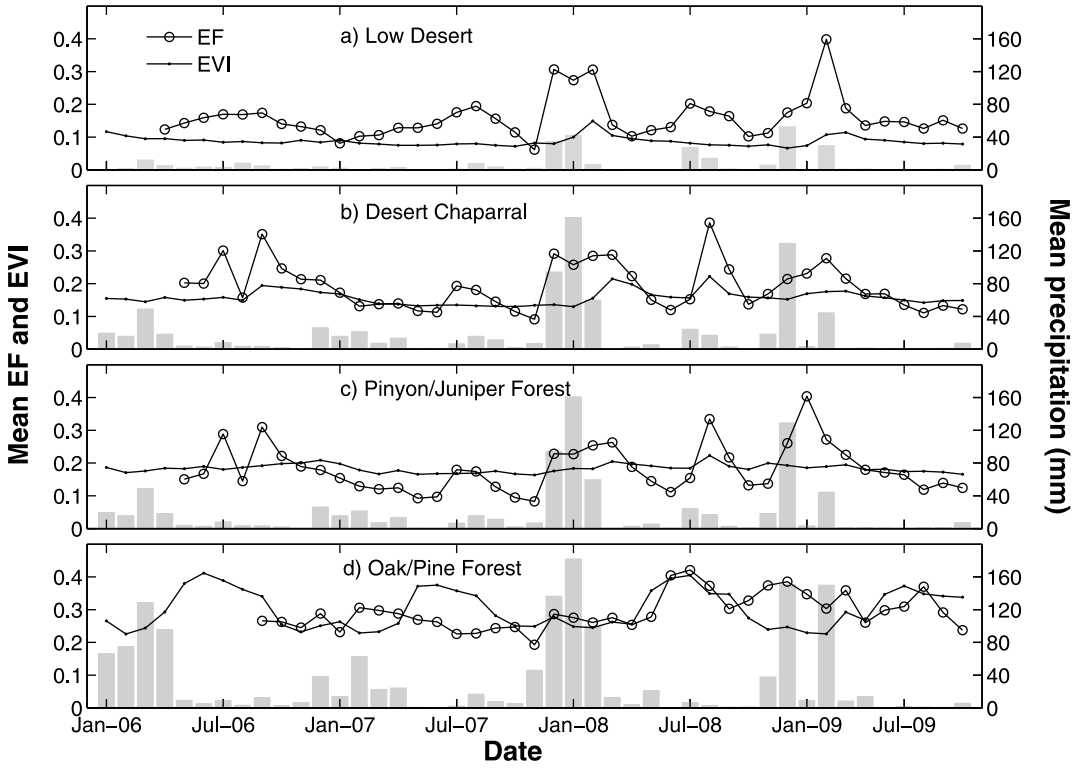

Figure 8. Monthly mean EF and 16 day EVI (left axis) and precipitation (right axis) for each eddy covariance tower site. Monthly mean tower EF was calculated from the mean of all valid, daytime half-hour EF measurements. Tower EF measurements go from the establishment of each tower until October 2009. EVI was obtained by averaging and weighting the 16 day MODIS data for the month from the pixel that contained each tower. Precipitation data were taken from the monthly PRISM data for the 4 km pixel containing each tower. All towers show good correlation between peak precipitation and EF, while the Oak/Pine tower shows the greatest variation in EVI.

significantly between classes with nonvegetative cover decreasing from ~60% in the Low Desert to 5% in the Deciduous Oak.

[25] Among classes, normal annual precipitation increases from 240 mm for the Low Sonoran Desert to 613 mm for the Live Oak and Conifer (Evergreen). January has highest mean precipitation ranging from ~60 mm month^{-1} in the Low Desert to ~140 mm month^{-1} in the Evergreen class (Figure 6). June has the lowest precipitation with all classes averaging less than 10 mm month^{-1}. The pattern and rank of each class remains relatively constant during the rainiest months (January–March) with the exception of the Grassland and Mixed classes, which increases by one rank relative to the other seven classes in February and March, respectively. Summer precipitation associated with the North American monsoon contributes less than 20% to the mean annual precipitation. The desert classes receive ~15%, and all other classes receive 10–11% of their annual precipitation from July to August.

[26] Maximum mean monthly temperature occurs in July for all classes while January has minimum temperature (Figure 7). Mean temperature remains above freezing for all classes throughout the year though the Mixed and Evergreen classes have mean temperature lower than 5°C in January and February. Mean peak summer temperatures range from 21° to 29°C. The temperature rank of most classes remains constant throughout the year with the exception of the Grassland and Mixed classes. The monthly temperature range between the coldest and warmest vegetation classes is between 5° and 10°C, with June and July having the largest range and December the smallest.

3.2. Seasonal, Interannual, and Spatial Variation in Evaporative Fraction

[27] To assess controls on EF at longer timescales, we compared mean monthly EF, monthly precipitation, and EVI observed at the four EC towers in the study area from 2006 until October 2009 (Figure 8). At three of the towers (Low Desert, disturbed Open Shrubland, and undisturbed Open Shrubland), seasonal variation in EVI was less than 0.1 with jumps in EVI one to two months after significant (>25 mm month^{-1}) precipitation. The Oak/Pine tower showed greater variation in EVI, ranging from about 0.25 to 0.4 over 2006–2009. Maximum monthly precipitation ranged from ~55 mm month^{-1} in December 2008 at the Low Desert site to 180 mm month^{-1} in January 2008 at the Oak/Pine tower. Almost all precipitation fell during winter months (November–February).

[28] Precipitation was a major control on the mean annual EF with a moderate correlation (r = 0.47) between mean annual precipitation and EF and a much stronger correlation (r = 0.91) when the anomalous grassland class was excluded

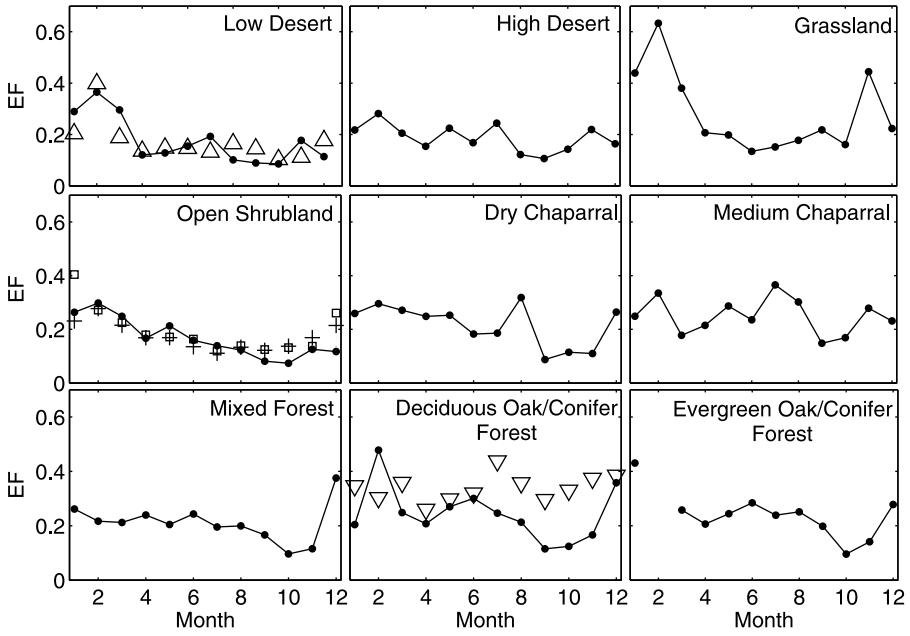

Figure 9. Monthly mean evaporative fraction (EF) for each class for each month of the REFEB sampling campaign. Mean EF is obtained by simple average of valid REFEB measurements for each month and class. Mean monthly EF for classes with eddy covariance (EC) towers (Low Desert, Open Shrubland, and Deciduous Oak) are shown as nonconnected symbols. Open Shrubland class has two EC towers in unburned (squares) and burned areas (pluses).

(data not plotted). Empirically, mean annual class EF (EF_{ma}) was related to precipitation by equation (3):

$$EF_{ma} = 4.29 \times 10^{-4} * pclass + 0.0936 \quad (3)$$

where pclass is mean annual class precipitation for the 2008–2009 water year. All EC tower sites saw increased EF following precipitation (Figure 8), but at the Low Desert and Undisturbed Open Shrubland tower, peaks in EF always occurred one to two months following significant precipitation, whereas the Oak/Pine tower also saw summer peaks in EF independent of precipitation for all years except the drought water year of 2006–2007. For the Oak/Pine tower, maximum seasonal EF usually coincided with peak EVI, indicating that transpiration is a major fraction of energy partitioning at this site. In the drought year of 2006–2007, there was a summer maximum in EVI without a corresponding increase in EF, indicating deciduous leaf out despite the lack of precipitation the preceding winter.

[29] Regional REFEB EF showed considerable seasonal and spatial variation (Figure 9). We obtained valid EF measurements from REFEB for every month and class except February in Live Oak/Conifer, when snow precluded access. With the exception of Evergreen, all of the classes that occurred on one side of the mountain (desert, grassland, open Shrubland, and deciduous oak) had the highest EF in February following precipitation, with maximum EF ranging from ~0.3 (Upper Desert and Open Shrubland) to 0.63 (Grassland). The dry and medium chaparral/high pine classes had the highest EF in July and August, respectively, while the mixed chaparral, oak, and conifer had peak EF in December. The highest summer EF in the chaparral/high forest is due to the high-elevation (>2300 m) samples of these vegetation types in the Santa Rosa Mountains (Data Set S1). With the exception of grassland, all classes had their lowest monthly mean EF in either September or October, with minimum EF less than 0.15, before EF increases in November and/or December.

[30] With the exception of the Oak/Pine tower and December–January at the Open Shrubland towers, the eddy

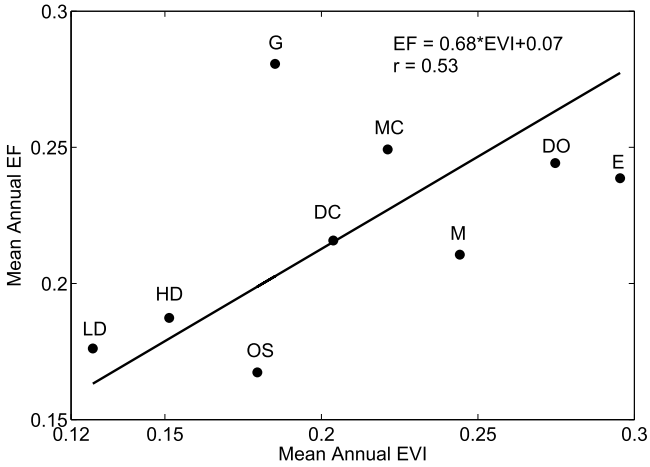

Figure 10. Mean annual EF for each vegetation class regressed against mean annual EVI for REFEB measurements within that class. Regression between mean EVI and EF was calculated using geometric mean regression. Grassland and Open Shrubland are the two ecosystems that show large deviations from the trend of higher ecosystem/precipitation/EVI and higher EF.

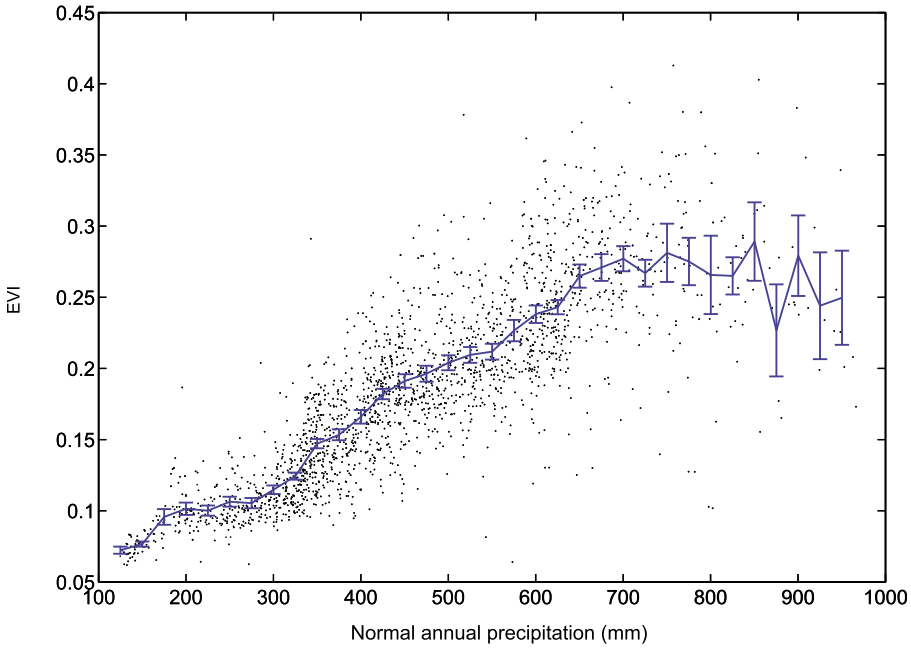

Figure 11. Normal annual precipitation versus mean EVI for each pixel in Figure 8 maps and 25 mm bins of mean precipitation and 3 times standard error (bars). Binned data show significant step changes in the mean precipitation:EVI relationship between 150 and 175 mm, 350 and 375 mm, and 650 and 675 mm precipitation.

covariance (EC) towers' mean monthly EF closely matched the REFEB observations of mean monthly EF in the vegetation class in which the tower was located (Figure 9). The absolute mean difference between the monthly EF for the towers and the respective REFEB EF measurements ranged from 0.050 to 0.123. The correlation between monthly mean EF between the EC towers and REFEB platform gives confidence that REFEB accurately observes the magnitude and seasonality of EF in vegetation classes where there is no EC tower.

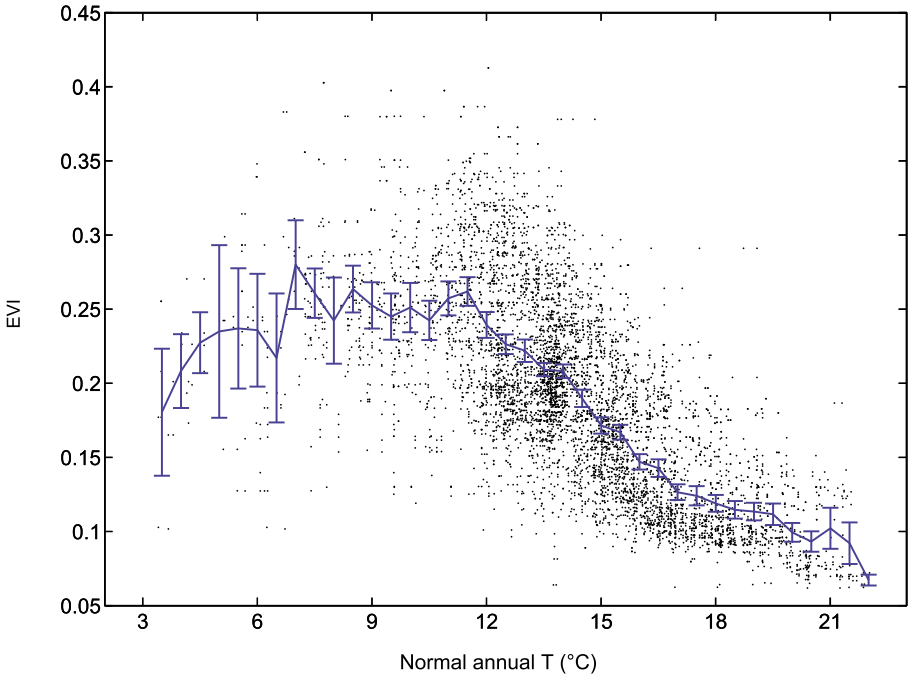

Figure 12. Normal annual temperature versus mean EVI for each pixel in Figure 8 maps and 0.5°C of mean temperature and 3 times standard error (bars). Binned data show significant decrease in the mean temperature:EVI relationship between 14.5° and 16.5°C.

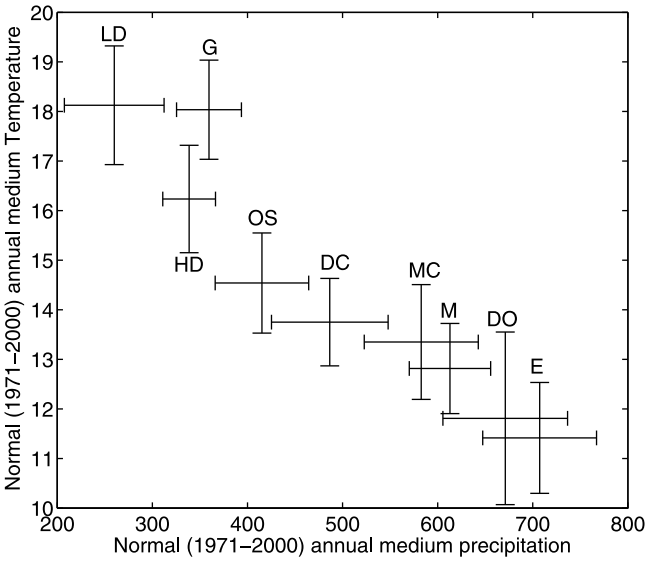

Figure 13. Climate space for each ENVI vegetation class. Bars show class medium and interquartile range for temperature and precipitation for locations in each class.

[31] Annually averaged EF generally increased with higher, more vegetated classes (Figure 10) with the exception of Grassland and Open Shrubland. Mean annual EF was correlated with mean EVI (r = 0.53), with a significantly larger correlation (r = 0.81) if the outlying grassland class is excluded. We initially hypothesized that the high annual EF for the grassland was due to the influence of February's EF (EF > 0.6) during a month with less insolation; however, weighting the monthly mean EF by average incoming solar radiation (not shown) measured at our EC towers still resulted in Grassland having the highest mean annual EF and Open Shrubland having the lowest. The correlation between mean annual EVI and EF improved slightly (r = 0.60) when monthly EF was weighted by insolation. At intra-annual timescales, 16 day EVI was a poor predictor of EF at individual sites. Of all of our vegetation classes, EVI predicted instantaneous EF moderately well (r = 0.49) in grasslands. In all other classes, the correlation coefficient was less than 0.20.

3.3. Relationship Between Climate and Vegetation Across Elevational Gradients

[32] Precipitation has a strong positive correlation with EVI (Figure 11), and temperature has a strong negative correlation with EVI (Figure 12). EVI increases with normal annual precipitation from about ~125 to 650 mm yr^{-1}, with several sharp changes. To analyze the robustness of these nonlinear changes, we plotted the mean EVI and ±3 times standard error (SE) in 25 mm precipitation bins (Figure 11). Significant step changes in the mean relationship between precipitation and EVI (defined by nonoverlapping error bars between adjacent precipitation bins) occurred between 150 and 175 mm, 325 and 350 mm, 375–425 mm, 575 and 600 mm, and 650 and 675 mm. Uncertainty in mean EVI for each precipitation bin was less than 0.02 for all bins less than 700 mm, but increased for higher-precipitation classes.

[33] EVI decreases with increasing temperature above a mean normal temperature of 12°C, with fewer sharp changes than the precipitation-EVI relation (Figure 12). Again we plotted mean and ±3 times SE. In 0.5°C bins. There was no significant step change in the mean temperature EVI relationship between 3.5° and 11.5°C, though the temperature-EVI relation increased significantly between 3.5° and 7°C. In the individual pixel relations between precipitation-EVI (Figure 11) and temperature-EVI (Figure 12), there were numerous pixels at colder and wetter locations that have significantly below average EVI.

[34] We plotted the median and interquartile range of class precipitation versus temperature to assess the relative impact of these climate variables on controlling vegetation class distribution (Figure 13). With respect to precipitation, most classes had overlapping ranges with two or fewer other classes. With respect to temperature, there was more overlap with most classes sharing climate space with three to five other classes. The Low Desert-Grassland, Medium Chaparral-Mixed, and Deciduous-Evergreen Oak and Conifer classes had a median temperature within 0.5°C of each other.

4. Discussion

4.1. Uncertainties in REFEB and EC Observations of EF

[35] REFEB has similar assumptions and likely has similar errors as other Bowen Ratio type approaches [*Anderson and Goulden*, 2009]. The key requirement for REFEB, and the T′-q′ Regression Bowen Ratio Method, is observation of Monin-Obukhov Similarity Theory (MOST) [*De Bruin et al.*, 1999]. MOST can be assessed by taking the correlation coefficient between T′ and q′ (rTQ); if rTQ = 1, then MOST must be observed [*De Bruin et al.*, 1999]. When rTQ is significantly less than one, MOST may or may not be observed. *De Bruin et al.* [1999] presented experimental micrometeorological evidence that showed that MOST was observed when rTQ was greater than 0.25. At a micrometeorological tower in California, *Anderson and Goulden* [2009] also found good agreement between EF calculated using the T′-q′ regression and eddy covariance methods when rTQ was greater than 0.25.

[36] Eddy covariance (EC) measurements in mountainous terrain have been challenging due to the impact of topography on mechanical airflow [*Hammerle et al.*, 2006]. However, multiple EC towers in mountainous landscapes [e.g., *Turnipseed et al.*, 2003; *Hammerle et al.*, 2006; *Hiller et al.*, 2008] have found that EC measurements during typical daytime mountainous conditions (upslope airflow and active turbulence) have uncertainties similar to less complex terrain as assessed by energy budget closure. These studies cover both short canopy (grassland) and tall canopy (conifer forest) ecosystems. We believe that our filters for including EC measurements ensure that we analyze measurements made during typical conditions. Furthermore, monthly REFEB EF from the classes that included EC towers had good agreement against their respective towers. This convergence in EF, with different methods that rely on different assumptions of atmospheric transport, supports the accuracy of both REFEB and EC for daytime measurements. Based on this convergence, we assume that study area daytime REFEB and EC measurements have similar errors as regions with simpler terrain, where errors for both Bowen Ratio type measurements [e.g., *Sinclair et al.*, 1975; *Angus and Watts*, 1984; *Heilman et al.*, 1989; *Perez et al.*, 1999] and eddy covariance

[e.g., *Goulden et al.*, 1996; *Finkelstein and Sims*, 2001; *Baldocchi*, 2003] are well documented.

4.2. Temporal and Spatial Patterns of Energy Exchange and Their Relationship to Vegetation and Climate

[37] Annual class EF during the 2008–2009 water year varied by only 0.11 (from 0.17 to 0.28), which was significantly less than the relative variation in precipitation (81–575 mm). This difference indicates that significant spatial variation in net radiation and available energy enhances or suppresses the actual ET across the study area. Areas with higher vegetation cover have five properties that increase net radiation and available energy. First, they have lower albedos and absorb more incoming solar radiation [e.g., *Baldocchi et al.*, 2004]. We observed this relationship between higher vegetation cover and lower albedo (Figure 3). Second, they have higher surface roughness that results in more effective transfer of sensible heat energy from the surface to the atmosphere, resulting in a cooler surface that reduces outgoing longwave radiation. In a transition from open shrubland to semiarid forest, *Rotenberg and Yakir* [2010] found that greater surface roughness increased net radiation by about the same amount (~25 W m^{-2}) as decreased albedo, with the forest ecosystem absorbing ~50 W m^{-2} more than the shrubland. Third, ground heat fluxes in forests are significantly less than in open canopy ecosystems such as shrublands, deserts, and grasslands, thus increasing available energy [e.g., *Oliver et al.*, 1987]. Fourth, more vegetated classes occur at higher elevations where incoming solar radiation is greater due to decreased atmospheric absorption [*Schroeder et al.*, 2009]. Fifth, surface air temperatures are lower, reducing outgoing longwave radiation. Increased available energy in more vegetated classes is likely to increase with precipitation and ET, thus resulting in less relative change in mean EF between classes despite large differences in water availability.

[38] Precipitation was the dominant influence on the temporal patterns of EF patterns in lower-elevation ecosystems (Deserts, Grasslands, and Open Shrubland). 50% or more of their area was either not vegetated or was in deciduous shrub or grass (Table 3) with an LAI of less than 2. Higher-elevation ecosystems (Chaparral and Forests) had more cover and LAI greater than 2, suggesting that transpiration from deeper rooted, summer active, species could contribute more to EF patterns in these classes, as opposed to the bare soil evaporation and short-lived low-elevation deciduous plants that respond more quickly to significant rainfall. The reduced transpiration at lower elevations may mean that a greater percentage of precipitation runs off or deeply infiltrates the soil. Studies in other semiarid regions such as the Sahel have shown an increase in the height of the groundwater table despite decreasing precipitation and severe droughts due to increased runoff and selective recharge [*Leduc et al.*, 2001]. *Boulain et al.* [2009] showed that relative recharge and runoff in the Sahel were considerably more variable than rainfall; low vegetation cover enabled high recharge in wet years due to a lack of vegetation that could access deeper moisture. This sustained runoff and increase in relative water yield may reduce the impact on groundwater and surface runoff for downstream users and ecosystems.

[39] While climate and vegetation have the largest controls on EF, topography can have major local impacts. For example, the Deciduous Oak and Pine tower is in a locally wet area; it is in a valley with a flux footprint primarily in or near a creek bed where deciduous oaks can access water into the fall during years with normal or above average precipitation. The tower does not exhibit the fall minimum in EF like the other towers and most of the REFEB measurements. We believe this accounts for the discrepancy between REFEB and EC EF measurements in the Deciduous Oak class (Figure 9). Another example is the presence of high-elevation cold and wet pixels that have significantly below average EF. We believe this is due to the presence of rocky outcrops and ridges at higher elevations and along the very steep (slope >40°) north face of San Jacinto Peak (Figure 2a) that are not vegetated due to a lack of soil.

4.3. Vegetation Indexes as Assessors of EF in Montane Ecosystems

[40] Vegetation Indices (VIs) ability to predict EF in semiarid regions depends on ecosystem type. Some studies [e.g., *Nagler et al.*, 2005, 2007; *Wang and Liang*, 2008] have found a strong relationship ($r > 0.7$) between EVI and ET and EF at daily monthly timescales. Studies in other Mediterranean ecosystems similar to the study area have found results similar to ours; NDVI and EVI remain relatively constant while transpiration and photosynthesis show large seasonal variation [*Garbulsky et al.*, 2008]. The weak EVI-EF relationship at intra-annual timescales in most of the study area's classes severely limits the ability of using EVI to estimate regional ET. Furthermore, the elevational heterogeneity confounds the use of temperature or temperature-VI metrics [e.g., *Carlson*, 2007; *Wang and Liang*, 2008] to assess regional ET [*Li et al.*, 2009].

[41] Despite its inability to predict seasonal dynamics of energy partitioning in the study area, EVI may be useful for evaluating interannual changes in EF. In the study area, mean annual EVI and EF are moderately correlated at the class level ($r > 0.50$) at both the tower (Figure 8) and REFEB platform (Figure 10). Over longer timescales, EVI may be an even better predictor of a location's mean annual EF due to the linkage between precipitation and vegetation (Figure 11). In other Mediterranean-type ecosystems, NDVI is well correlated to interannual variability in precipitation [*Maselli*, 2004]. Other indices such as the Normalized Differential Water Index (NDWI) may work better in assessing the water state and ET in the study area [*Gao*, 1996; *Dennison et al.*, 2005].

4.4. Controls on Vegetation Distribution

[42] Across the study area, the greatest vegetation changes occurred in areas with mean annual temperatures between 12° and 16.5°C and annual precipitation between 300 and 425 mm and 550–650 mm (Figures 12 and 11). These regions overlap to a considerable extent (Figures 2b and 2c); we would expect to see the largest shift in vegetation in these regions for a given change in precipitation or temperature. The step changes in EVI with precipitation are likely due to vegetation communities not being able to survive past a climatic limit. For example, on the windward side, chaparral species such as chamise (*Adenostoma fasciculatum*) and manzanita (*Arctostaphylos* spp) generally require more than 300 mm of annual precipitation [*Westman*, 1991]. On the leeward side, Pinyon Pine (*Pinus edulis monophyla*-type),

has a mean annual precipitation requirement of about 500 mm and a minimum requirement of ~170 mm [*Cole et al.*, 2007]. Pinyon in the study area, which occurs exclusively in the Open Shrubland class, is already below this mean (Figure 2b) and has been subjected to precipitation means near or below the minimum requirement during the 2008–2009 and 2006–2007 water years (Figures 8b and 8c).

[43] At higher elevations, live oak and conifer are found on both the east and west side of the study area beginning at ~625–650 mm precipitation; these vegetation types do not occur below that precipitation limit unless they are in a valley and obtain supplemental water from a stream. However, the mean annual temperature at the ~650 mm yr^{-1} precipitation level is 9°–12°C on the leeward slope (Santa Rosa/El Toro), while it is 12°–15°C on the windward slope of San Jacinto. The presence of significant forest die back on both slopes of the study area under different temperatures underscores the importance of precipitation as a primary control on plant distribution and ecosystem shifts [*Kelly and Goulden*, 2008; *USDA*, 2007].

[44] With respect to controls on vegetation distribution, three observations support the case that precipitation is more important than temperature. First, there are two class pairs (Low Desert-Grassland and Deciduous Oak/Conifer-Live Oak/Conifer) that have median temperatures that differ by less than 0.25°C but have median precipitation that differs by 50 mm or more (Figure 13). Second, classes that have similar timing of peak EVI (Figure 5) and mean monthly temperatures (Figure 7) that differ by less than 2°C in all months (Deserts and Grassland), have significantly different mean EVI values. In these classes the greater relative difference between classes is in monthly class precipitation (Figure 6). Third, there are three classes whose precipitation range overlaps with three other classes, while there are five classes whose temperature range overlaps with four or five other classes (Figure 13). Temperature changes may control vegetation and energy partitioning by altering the location of winter and summer photosynthesis. For example, the break between the Grassland and Open Shrubland classes (Figure 13) might indicate that temperature controls the distribution of winter active vegetation. The Grassland and Desert classes have EVI that peak prior to April (Figure 5). These classes have monthly mean temperatures that were always warmer than 8°C, which indicate sufficiently warm temperatures for winter photosynthesis (Figure 7).

4.5. Potential Impacts of Climate Change on Vegetation and Energy Partitioning

[45] Predicted climate change (warmer and drier [e.g., *Seager et al.*, 2007; *Diffenbaugh et al.*, 2008]) may alter energy partitioning and ET in the study area by reducing vegetation cover and changing the mean and seasonality of EF (Figure 10) and available energy. Multiple mechanisms have been observed in southern California to facilitate reduced vegetation cover. First, increased severity of wildfire may stress longer-lived chaparral and shrub species, resulting in a transition to ecosystems (such as grasslands) with a faster fire return interval [*Syphard et al.*, 2007]. Second, severe droughts, such as the 2001–2002 and 2006–2007 droughts, lead to cavitation that can result in plant injury or death [*Jacobsen et al.*, 2007]. Furthermore, plants that are more fire-adapted show less resilience and resistance to cavitation [*Jacobsen et al.*, 2007]. Third, water deficits due to less precipitation and greater evaporative demand can lead to plant stomatal closure, eventually resulting in a "carbon starvation" that can weaken vegetation to pathogens (e.g., bark beetle) [*Breshears et al.*, 2009].

[46] While evaluation of the relative importance of these mechanisms is beyond the scope of this study, we consider observed vegetation shifts and their impact on energy partitioning. *Kelly and Goulden* [2008] found that vegetation shifted upward in a "lean" pattern where lower-elevation individuals of a species died out without recruitment of new individuals at new locations at or above the upper limit of a species range. This finding contradicts previous ecological assumptions that plant species would "march" upslope uniformly in response to warming climate [*Breshears et al.*, 2008]. Several reasons may account for this "lean" pattern. *Kelly and Goulden* [2008] found that precipitation variability was significantly larger in elevational terms than other climate variables. Precipitation variability inhibit establishment in xeric environments; some species may require sustained pluvial periods to grow enough to withstand drought [e.g., *Laura Suarez and Kitzberger*, 2010]. A second reason may be due to a lack of soil development that hinders upslope movement. *Hanawalt and Whittaker* [1976] found greatest soil organic content and nutrient availability at mid elevation sites in the study area. Upslope locations may have suitable water availability in a future climate, but could lack necessary soil properties to support plant communities found at lower elevations, thus hindering vegetation movement. Assuming that this lean pattern holds across the study area with future change, the distribution and relative prevalence of winter and summer dominant species may change, affecting the seasonality of and reducing annual average EF. While it should be noted that *Kelly and Goulden* [2008] did not find changes in the overall amount of cover in their study, their results are consistent with current understanding of montane ecological responses to climate change [*Adams et al.*, 2009].

5. Conclusion

[47] We measured seasonal and spatial patterns of energy partitioning across a semiarid montane climate gradient in southern California and related these patterns to larger-scale changes in climate and vegetation. The tower data show that precipitation timing is the largest control on energy partitioning at lower-elevation ecosystems while higher-elevation systems are more controlled by vegetation. Step changes in the precipitation-EVI relationship suggest that energy partitioning could change as a result of a warmer and drier future climate. Comparison among the mean class temperature and precipitation suggests that precipitation has a greater control on vegetation distribution and thus energy partitioning than temperature.

[48] Given the role of southern California's mountains in regional water supplies, predicting change in precipitation, vegetation, energy partitioning, and available energy is key to understanding how regional hydrology will change under future climate change. Our study was the first to directly measure regional relationships between energy partitioning, precipitation, temperature, and vegetation in this heterogeneous region. In order to predict future change

and to understand its mechanisms, we need to combine high-resolution climate and biogeochemical modeling with field data.

[49] **Acknowledgments.** We thank Aaron Fellows, Jim Randerson, and Jay Famiglietti for their ideas and feedback on the paper. The University of California James San Jacinto Mountain Reserve and its staff, Rebecca Fenwick and Taylor Jeffrey, graciously provided logistical support for the field measurements. Precipitation and temperature data were graciously provided by the University of California Phillip J. Boyd Deep Canyon Desert Research Center and its staff, Mark Fisher and Allan Muth. We thank the editor, Dennis Baldocchi, associate editor, and two anonymous reviewers for their comments and suggestions. This study was funded by the U.S. Department of Energy and NASA. Ray Anderson was supported by a Ralph and Carol Cicerone Fellowship at UC Irvine.

References

Adams, H. D., M. Guardiola-Claramonte, G. A. Barron-Gafford, J. C. Villegas, D. D. Breshears, C. B. Zou, P. A. Troch, and T. E. Huxman (2009), Temperature sensitivity of drought-induced tree mortality portends increased regional die-off under global-change-type drought, *Proc. Natl. Acad. Sci. U. S. A.*, *106*, 7063–7066, doi:10.1073/pnas.0901438106.

Anderson, R. G., and M. L. Goulden (2009), A mobile platform to constrain regional estimates of evapotranspiration, *Agric. For. Meteorol.*, *149*, 771–782, doi:10.1016/j.agrformet.2008.10.022.

Angus, D. E., and P. J. Watts (1984), Evapotranspiration—How good is the Bowen ratio method?, *Agric. Water Manage.*, *8*(1–3), 133–150, doi:10.1016/0378-3774(84)90050-7.

Baldocchi, D. D. (2003), Assessing the eddy covariance technique for evaluating carbon dioxide exchange rates of ecosystems: Past, present and future, *Global Change Biol.*, *9*, 479–492, doi:10.1046/j.1365-2486.2003.00629.x.

Baldocchi, D. D., L. Xu, and N. Kiang (2004), How plant functional-type, weather, seasonal drought, and soil physical properties alter water and energy fluxes of an oak-grass savanna and an annual grassland, *Agric. For. Meteorol.*, *123*, 13–39, doi:10.1016/j.agrformet.2003.11.006.

Bastiaanssen, W., M. Menenti, R. Feddes, and A. Holtslag (1998), A remote sensing surface energy balance algorithm for land (SEBAL). 1. Formulation, *J. Hydrol.*, *212–213*, 198–212, doi:10.1016/S0022-1694(98)00253-4.

Beringer, J., F. Chapin, C. Thompson, and A. Mcguire (2005), Surface energy exchanges along a tundra-forest transition and feedbacks to climate, *Agric. For. Meteorol.*, *131*, 143–161, doi:10.1016/j.agrformet.2005.05.006.

Betts, R. A., P. M. Cox, S. E. Lee, and F. I. Woodward (1997), Contrasting physiological and structural vegetation feedbacks in climate change simulations, *Nature*, *387*, 796–799, doi:10.1038/42924.

Bonfils, C., et al. (2008), Detection and attribution of temperature changes in the mountainous western United States, *J. Clim.*, *21*, 6404–6424, doi:10.1175/2008JCLI2397.1.

Boulain, N., B. Cappelaere, L. Séguis, G. Favreau, and J. Gignoux (2009), Water balance and vegetation change in the Sahel: A case study at the watershed scale with an eco-hydrological model, *J. Arid Environ.*, *73*, 1125–1135, doi:10.1016/j.jaridenv.2009.05.008.

Breshears, D. D., et al. (2005), Regional vegetation die-off in response to global-change-type drought, *Proc. Natl. Acad. Sci. U. S. A.*, *102*, 15,144–15,148, doi:10.1073/pnas.0505734102.

Breshears, D. D., T. E. Huxman, H. D. Adams, C. B. Zou, and J. E. Davison (2008), Vegetation synchronously leans upslope as climate warms, *Proc. Natl. Acad. Sci. U. S. A.*, *105*, 11,591–11,592, doi:10.1073/pnas.0806579105.

Breshears, D. D., O. B. Myers, C. W. Meyer, F. J. Barnes, C. B. Zou, C. D. Allen, N. G. McDowell, and W. T. Pockman (2009), Tree die-off in response to global change-type drought: Mortality insights from a decade of plant water potential measurements, *Front. Ecol. Environ*, *7*, 185–189, doi:10.1890/080016.

Carlson, T. (2007), An overview of the "triangle method" for estimating surface evapotranspiration and soil moisture from satellite imagery, *Sensors*, *7*, 1612–1629, doi:10.3390/s7081612.

Cole, K. L., J. Fisher, S. T. Arundel, J. Cannella, and S. Swift (2007), Geographical and climatic limits of needle types of one- and two-needled pinyon pines, *J. Biogeogr.*, *35*, 257–269, doi:10.1111/j.1365-2699.2007.01786.x.

Cramer, W., et al. (2001), Global response of terrestrial ecosystem structure and function to CO2 and climate change: Results from six dynamic global vegetation models, *Global Change Biol.*, *7*, 357–373, doi:10.1046/j.1365-2486.2001.00383.x.

De Bruin, H. A. R., B. J. J. M. Van Den Hurk, and L. J. M. Kroon (1999), On the temperature-humidity correlation and similarity, *Boundary Layer Meteorol.*, *93*, 453–468, doi:10.1023/A:1002071607796.

Dennison, P. E., D. A. Roberts, S. H. Peterson, and J. Rechel (2005), Use of normalized difference water index for monitoring live fuel moisture, *Int. J. Remote Sens.*, *26*, 1035–1042, doi:10.1080/01431160420002739 98.

Diffenbaugh, N. S., F. Giorgi, and J. S. Pal (2008), Climate change hotspots in the United States, *Geophys. Res. Lett.*, *35*, L16709, doi:10.1029/2008GL035075.

Evrendilek, F., and O. Gulbeyaz (2008), Deriving vegetation dynamics of natural terrestrial ecosystems from MODIS NDVI/EVI data over Turkey, *Sensors*, *8*, 5270–5302, doi:10.3390/s8095270.

Ezzahar, J., A. Chehbouni, J. C. B. Hoedjes, and A. Chehbouni (2007), On the application of scintillometry over heterogeneous grids, *J. Hydrol.*, *334*, 493–501, doi:10.1016/j.jhydrol.2006.10.027.

Finkelstein, P. L., and P. F. Sims (2001), Sampling error in eddy correlation flux measurements, *J. Geophys. Res.*, *106*, 3503–3509, doi:10.1029/2000JD900731.

Friedl, M. A., et al. (2002), Global land cover mapping from MODIS: Algorithms and early results, *Remote Sens. Environ.*, *83*, 287–303, doi:10.1016/S0034-4257(02)00078-0.

Gao, B. C. (1996), NDWI—A normalized difference water index for remote sensing of vegetation liquid water from space, *Remote Sens. Environ.*, *58*, 257–266, doi:10.1016/S0034-4257(96)00067-3.

Garbulsky, M. F., J. Penuelas, D. Papale, and I. Filella (2008), Remote estimation of carbon dioxide uptake by a Mediterranean forest, *Global Change Biol.*, *14*, 2860–2867, doi:10.1111/j.1365-2486.2008.01684.x.

Goulden, M. L., J. W. Munger, S. Fan, B. C. Daube, and S. C. Wofsy (1996), Measurements of carbon sequestration by long-term eddy covariance: Methods and a critical evaluation of accuracy, *Global Change Biol.*, *2*, 169–182, doi:10.1111/j.1365-2486.1996.tb00070.x.

Goulden, M. L., G. C. Winston, A. M. S. McMillan, M. E. Litvak, E. L. Read, A. V. Rocha, and J. R. Elliot (2006), An eddy covariance mesonet to measure the effect of forest age on land-atmosphere exchange, *Global Change Biol.*, *12*, 2146–2162, doi:10.1111/j.1365-2486.2006.01251.x.

Hammerle, A., A. Haslwanter, M. Schmitt, M. Bahn, U. Tappeiner, A. Cernusca, and G. Wohlfahrt (2006), Eddy covariance measurements of carbon dioxide, latent and sensible energy fluxes above a meadow on a mountain slope, *Boundary Layer Meteorol.*, *122*, 397–416, doi:10.1007/s10546-006-9109-x.

Hanawalt, R. B., and R. H. Whittaker (1976), Altitudinally coordinated patterns of soils and vegetation in-the San Jacinto Mountains, California, *Soil Sci.*, *121*, 114–121, doi:10.1097/00010694-197602000-00007.

Heilman, J., C. Brittin, and C. Neale (1989), Fetch requirements for bowen ratio measurements of latent and sensible heat fluxes, *Agric. For. Meteorol.*, *44*(3–4), 261–273, doi:10.1016/0168-1923(89)90021-X.

Hidalgo, H. G., et al. (2009), Detection and attribution of streamflow timing changes to climate change in the western United States, *J. Clim.*, *22*, 3838–3855, doi:10.1175/2009JCLI2470.1.

Hiller, R., M. J. Zeeman, and W. Eugster (2008), Eddy-covariance flux measurements in the complex terrain of an alpine valley in Switzerland, *Boundary Layer Meteorol.*, *127*, 449–467, doi:10.1007/s10546-008-9267-0.

Hogg, E. H., D. T. Price, and T. A. Black (2000), Postulated feedbacks of deciduous forest phenology on seasonal climate patterns in the western Canadian interior, *J. Clim.*, *13*, 4229–4243, doi:10.1175/1520-0442(2000)013<4229:PFODFP>2.0.CO;2.

Huete, A., K. Didan, T. Miura, E. P. Rodriguez, X. Gao, and L. G. Ferreira (2002), Overview of the radiometric and biophysical performance of the MODIS vegetation indices, *Remote Sens. Environ.*, *83*, 195–213, doi:10.1016/S0034-4257(02)00096-2.

Huxman, T. E., B. P. Wilcox, D. D. Breshears, R. L. Scott, K. A. Snyder, E. E. Small, K. Hultine, W. T. Pockman, and R. B. Jackson (2005), Ecohydrological implications of woody plant encroachment, *Ecology*, *86*, 308–319, doi:10.1890/03-0583.

Jacobsen, A. L., R. B. Pratt, F. W. Ewers, and S. D. Davis (2007), Cavitation resistance among 26 chaparral species of southern California, *Ecol. Monogr.*, *77*, 99–115, doi:10.1890/05-1879.

Jeton, A. E., S. A. Watkins, T. J. Lopes, and J. Huntington (2005), Evaluation of precipitation estimates from PRISM for the 1961–90 and 1971–2000 data sets, Nevada, *U.S. Geol. Surv. Sci. Invest. Rep.*, *2005–5291*. (Available at http://pubs.usgs.gov/sir/2005/5291/, accessed 24 Oct. 2010)

Karl, T. R., and K. E. Trenberth (2003), Modern global climate change, *Science*, *302*, 1719–1723, doi:10.1126/science.1090228.

Keeley, J. E., C. J. Fotheringham, and M. Morais (1999), Reexamining fire suppression impacts on brushland fire regimes, *Science*, *284*, 1829–1832, doi:10.1126/science.284.5421.1829.

Kelly, A. E., and M. L. Goulden (2008), Rapid shifts in plant distribution with recent climate change, *Proc. Natl. Acad. Sci. U. S. A.*, *105*, 11,823–11,826, doi:10.1073/pnas.0802891105.

Kleissl, J., S. Hong, and J. M. H. Hendrickx (2009), New Mexico Scintillometer Network: Supporting remote sensing and hydrologic and meteorological models, *Bull. Am. Meteorol. Soc.*, *90*, 207, doi:10.1175/2008BAMS2480.1.

LaDochy, S., R. Medina, and W. Patzert (2007), Recent California climate variability: Spatial and temporal patterns in temperature trends, *Clim. Res.*, *33*, 159–169, doi:10.3354/cr033159.

Laura Suarez, M., and T. Kitzberger (2010), Differential effects of climate variability on forest dynamics along a precipitation gradient in northern Patagonia, *J. Ecol.*, *98*, 1023–1034, doi:10.1111/j.1365-2745.2010.01698.x.

Law, B. E., et al. (2002), Environmental controls over carbon dioxide and water vapor exchange of terrestrial vegetation, *Agric. For. Meteorol.*, *113*, 97–120, doi:10.1016/S0168-1923(02)00104-1.

Leduc, C., G. Favreau, and P. Schroeter (2001), Long-term rise in a Sahelian water-table: The continental terminal in south-west Niger, *J. Hydrol.*, *243*, 43–54, doi:10.1016/S0022-1694(00)00403-0.

Li, Z.-L., R. Tang, Z. Wan, Y. Bi, C. Zhou, B. Tang, G. Yan, and X. Zhang (2009), A review of current methodologies for regional evapotranspiration estimation from remotely sensed data, *Sensors*, *9*, 3801–3853, doi:10.3390/s90503801.

Liang, S., H. Fan, M. Chen, C. J. Shuey, C. Walthall, C. Daughtry, J. Morisette, C. Schaaf, and A. Strahler (2002), Validating MODIS land surface reflectance and albedo products: Methods and preliminary results, *Remote Sens. Environ.*, *83*, 149–162, doi:10.1016/S0034-4257(02)00092-5.

Maselli, F. (2004), Monitoring forest conditions in a protected Mediterranean coastal area by the analysis of multiyear NDVI data, *Remote Sens. Environ.*, *89*, 423–433, doi:10.1016/j.rse.2003.10.020.

McKelvey, K. S., C. N. Skinner, C. Chang, D. C. Etman, S. J. Husari, D. J. Parsons, J. W. van Wagtendonk, and C. P. Weatherspoon (1996), An overview of fire in the Sierra Nevada, Sierra Nevada Ecosystem Project: Final report to Congress, vol. 2, Assessments and scientific basis for management options, Cent. for Water and Wildland Resour., Univ. of Calif., Davis.

McMillan, A. M. S., G. C. Winston, and M. L. Goulden (2008), Age-dependent response of boreal forest to temperature and rainfall variability, *Global Change Biol.*, *14*, 1904–1916, doi:10.1111/j.1365-2486.2008.01614.x.

Messerli, B., D. Viviroli, and R. Weingartner (2004), Mountains of the world: Vulnerable water towers for the 21(st) century, *Ambio*, *13*, 29–34.

Molotch, N. P., P. D. Brooks, S. P. Burns, M. Litvak, R. K. Monson, J. R. McConnell, and K. Musselman (2009), Ecohydrology controls on snowmelt partitioning in mixed-conifer sub-alpine forests, *Ecohydrology*, *2*, 129–142, doi:10.1002/eco.48.

Nagler, P. L., R. L. Scott, C. Westenberg, J. R. Cleverly, E. P. Glenn, and A. R. Huete (2005), Evapotranspiration on western U.S. rivers estimated using the Enhanced Vegetation Index from MODIS and data from eddy covariance and Bowen ratio flux towers, *Remote Sens. Environ.*, *97*, 337–351, doi:10.1016/j.rse.2005.05.011.

Nagler, P. L., E. P. Glenn, H. Kim, W. Emmerich, R. L. Scott, T. E. Huxman, and A. R. Huete (2007), Relationship between evapotranspiration and precipitation pulses in a semiarid rangeland estimated by moisture flux towers and MODIS vegetation indices, *J. Arid Environ.*, *70*, 443–462, doi:10.1016/j.jaridenv.2006.12.026.

Oliver, S., H. Oliver, J. Wallace, and A. Roberts (1987), Soil heat flux and temperature variation with vegetation, soil type and climate, *Agric. For. Meteorol.*, *39*, 257–269, doi:10.1016/0168-1923(87)90042-6.

Perez, P. J., F. Castellvi, M. Ibanez, and J. I. Rosell (1999), Assessment of reliability of Bowen ratio method for partitioning fluxes, *Agric. For. Meteorol.*, *97*, 141–150, doi:10.1016/S0168-1923(99)00080-5.

Pierce, D. W., et al. (2008), Attribution of declining western U.S. snowpack to human effects, *J. Clim.*, *21*, 6425–6444, doi:10.1175/2008JCLI2405.1.

Rannik, Ü., and T. Vesala (1999), Autoregressive filtering versus linear detrending in estimation of fluxes by the eddy covariance method, *Boundary Layer Meteorol.*, *91*, 259–280, doi:10.1023/A:1001840416858.

Rotenberg, E., and D. Yakir (2010), Contribution of semi-arid forests to the climate system, *Science*, *327*, 451–454, doi:10.1126/science.1179998.

Schaaf, C. B., et al. (2002), First operational BRDF, albedo and nadir reflectance products from MODIS, *Remote Sens. Environ.*, *83*, 135–148, doi:10.1016/S0034-4257(02)00091-3.

Scheffer, M., S. Carpenter, J. A. Foley, C. Folke, and B. Walker (2001), Catastrophic shifts in ecosystems, *Nature*, *413*(6856), 591–596, doi:10.1038/35098000.

Schroeder, T. A., R. Hember, N. C. Coops, and S. Liang (2009), Validation of solar radiation surfaces from MODIS and reanalysis data over topographically complex terrain, *J. Appl. Meteorol.*, *48*, 2441–2458, doi:10.1175/2009JAMC2152.1.

Scott, R. L., G. D. Jenerette, D. L. Potts, and T. E. Huxman (2009), Effects of seasonal drought on net carbon exchange from a woody-plant-encroached semiarid grassland, *J. Geophys. Res.*, *114*, G04004, doi:10.1029/2008JG000900.

Seager, R., et al. (2007), Model projections of an imminent transistion to a more arid climate in southwestern North America, *Science*, *316*, 1181–1184, doi:10.1126/science.1139601.

Serrano-Ortiz, P., A. S. Kowalski, F. Domingo, B. Ruiz, and L. Alados-Arboledas (2008), Consequences of uncertainties in CO_2 density for estimating net ecosystem CO_2 exchange by open-path eddy covariance, *Boundary Layer Meteorol.*, *126*, 209–218, doi:10.1007/s10546-007-9234-1.

Sinclair, T., L. Allen, and E. Lemon (1975), An analysis of errors in the calculation of energy flux densities above vegetation by a Bowen-ratio profile method, *Boundary Layer Meteorol.*, *8*, doi:10.1007/BF00241333.

Syphard, A. D., V. C. Radeloff, J. E. Keeley, T. J. Hawbaker, M. K. Clayton, S. I. Stewart, and R. B. Hammer (2007), Human influence on California fire regimes, *Ecol. Appl.*, *17*, 1388–1402, doi:10.1890/06-1128.1.

Tou, J. T., and R. C. Gonzalez (1974), *Pattern Recognition Principles*, 377 pp., Addison-Wesley, Reading, Mass.

Turnipseed, A. A., D. E. Anderson, P. D. Blanken, W. M. Baugh, and R. K. Monson (2003), Airflows and turbulent flux measurements in mountainous terrain Part 1. Canopy and local effects, *Agric. For. Meteorol.*, *119*, doi:10.1016/S0168-1923(03)00136-9.

U.S. Department of Agriculture (USDA) (2007), Environmental Assessment North Fork of the San Jacinto Healthy Forest Project, 109 pp., For. Serv., San Jacinto Ranger Dist., San Bernardino Natl. For., Riverside County, Calif.

van Mantgem, P. J., and N. L. Stephenson (2007), Apparent climatically induced increase of tree mortality rates in a temperate forests, *Ecol. Lett.*, *10*, 909–916, doi:10.1111/j.1461-0248.2007.01080.x.

Veenendaal, E. M., O. Kolle, and J. Lloyd (2004), Seasonal variation in energy fluxes and carbon dioxide exchange for a broad-leaved semi-arid savanna (Mopane woodland) in southern Africa, *Global Change Biol.*, *10*, 318–328, doi:10.1111/j.1365-2486.2003.00699.x.

Viviroli, D., and R. Weingartner (2004), The hydrological significance of mountains: From regional to global scale, *Hydrol. Earth Syst. Sci.*, *8*, 1017–1030, doi:10.5194/hess-8-1017-2004.

Wang, K. C., and S. L. Liang (2008), An improved method for estimating global evapotranspiration based on satellite determination of surface net radiation, vegetation index, temperature, and soil moisture, *J. Hydrometeorol.*, *9*, 712–727, doi:10.1175/2007JHM911.1.

Wendt, C. K., J. Beringer, N. J. Tapper, and L. B. Hutley (2007), Local boundary-layer development over burnt and unburnt tropical savanna: An observational study, *Boundary Layer Meteorol.*, *124*, 291–304, doi:10.1007/s10546-006-9148-3.

Westman, W. E. (1991), Measuring realized niche spaces: Climatic response of chaparral and coastal sage scrub, *Ecology*, *72*, 1678–1684, doi:10.2307/1940967.

R. G. Anderson, University of California Center for Hydrologic Modeling, University of California, 240L Rowland Hall, Irvine, CA 92697-4690, USA. (rganders@uci.edu)

M. L. Goulden, Department of Earth System Science, University of California, Irvine, CA 92697, USA. (mgoulden@uci.edu)